Soft Matter

www.rsc.org/softmatter

Volume 7 | Number 16 | 21 August 2011 | Pages 7125–7568

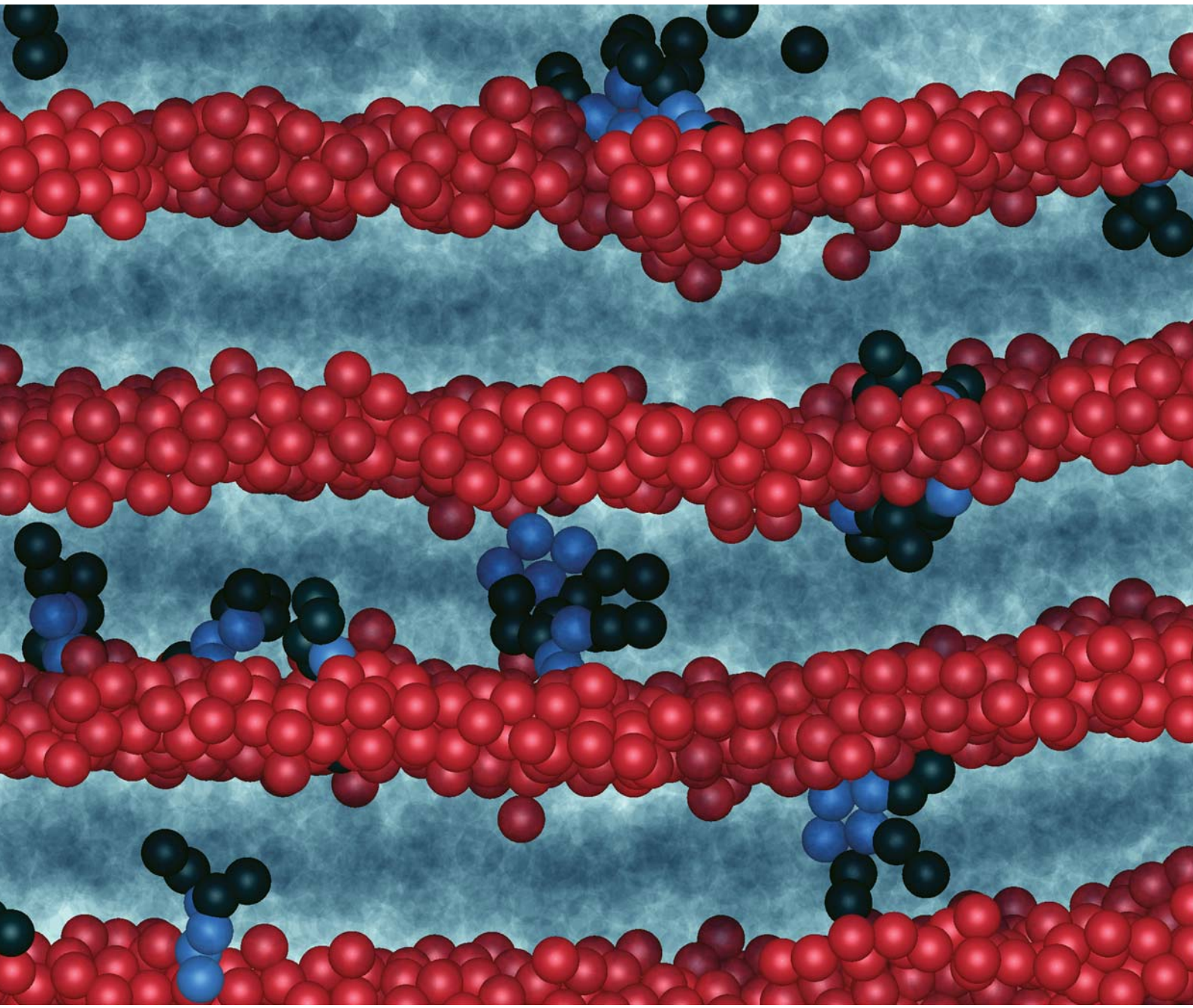

ISSN 1744-683X

RSC Publishing

PAPER

Erich A. Müller *et al.*

Global phase behaviour of polyphilic tapered dendrons

Soft Matter

Dynamic Article Links

Cite this: *Soft Matter*, 2011, **7**, 7465

www.rsc.org/softmatter

PAPER

Global phase behaviour of polyphilic tapered dendrons

Andrew J. Crane and Erich A. Müller*

Received 5th April 2011, Accepted 7th June 2011
DOI: 10.1039/c1sm05599b

We present a coarse-grained molecular dynamics study into the fluid phase behaviour of a model dendron like polyphilic molecule. Our model consists of 11 spherical beads, held in a semi flexible planar tapered arrangement, with a single apex bead and four interior beads defined to have self attraction, whilst the remaining periphery beads and all cross interactions are made softly repulsive, in essence bestowing an incompatibility between the three bead types. A parametric study was performed covering around 1000 state points in a domain of temperature and pressure spanning from regions where the fully isotropic fluid is observed, to the onset of crystallisation. Three micro-segregated thermotropic liquid crystalline phases are detected; a hexagonal columnar (HC) mesogenic phase, a supramolecular sphere body-centred cubic (SSbcc) mesogenic phase and a supramolecular sphere fluid (SSf) mesogenic phase. Each phase is characterized by order parameters based on dendron clustering distributions and spatial orientations, facilitating the phase diagram mapping. The mesogenic nature of the HC, SSbcc and SSf structured phases was confirmed visually, presenting dendron diffusion along and around the columns in the former, and intra and inter supramolecular sphere dendron diffusion in the latter two. HC and SSbcc phases were obtained by self-assembly by quenching from isotropic states, proving the stability and reproducibility of the liquid crystalline phases. Tracking of appropriate metrics gives insight into their formation mechanisms. Temperature driven first order phase transitions are seen from the HC phase to the SSf phase at higher pressures, and to the SSbcc and then SSf phase at lower pressures. For this latter transition, a Gibbs Duhem integration is used to trace the coexistence curve from a point determined by thermodynamic integration. The other transitions, including a continuous transition from the SSf to fully isotropic phase, are estimated from isothermal and isobaric simulation runs. It is of note that both the HC and SSbcc mesogenic phases resemble those reported experimentally however, the intermediate liquid-phase is an undiscovered prediction of our model. The simulations presented give physical insight on the relation between the apparent distinct phases observed. Our results shed light on the underlying relationships between these phases of self-organized supramolecular soft matter and showcase how the different experimental instances are local manifestations of an underlying generic phase diagram, which we present here.

1 Introduction

Although supramolecular organisation is ubiquitous throughout nature, it is only over the past half-century that the computational and experimental tools to study these phenomena have become available. The ability to induce self-assembly through the synthesis of designer compounds with clearly defined shapes and intermolecular interactions has been a central goal in material science, offering the promise of novel phases with highly tuneable properties.[1,2] A class of compounds of particular importance in this area are the polyphilic liquid crystals.[3–5] These molecules contain both the shape anisotropy that impart thermotropic liquid crystalline compounds with intermediate structural order,[6] and the required incompatibility at the level of short range molecular environments that drive local biomolecular self-assembly[7,8] or bulk phase separation.[9] Interplay of these qualities can induce spontaneous self-organisation of hierarchically structured periodic nanosegregated phases. Potential applications for these architectures are broad, and include roles in molecular transport control,[10] electronic[11] and biomimetic materials.[12] Many of these functions are reliant on material stimuli responsiveness, that arises from the same molecular mobility property that permits thermodynamically controlled self-assembly.

We focus in this report on a family of polyphilic dendron mesogens, that exhibit remarkable supramolecular thermotropic phases. These tree shaped compounds are characterised by three

Department of Chemical Engineering, Imperial College London, UK. E-mail: e.muller@imperial.ac.uk

distinct regions; a functionalised apex group, a shape-persistent core, and finally periphery units that confer the dendritic geometry. Typical apex groups range from simple methyl ester or carboxylic groups to more complex functionalities such as crown ethers, short peptides or polypodands. Periphery groups are normally alkyl chains or their fluorinated analogues, whilst the core sections are generally based on the benzyl ether units. Two example dendrons compounds are given in Fig. 1. Phase characterisation of these compounds, by differential scanning calorimetry, thermal optical polarised microscopy, X-ray diffraction and/or electron diffraction, indicate that they may form mesogenic structures of micro-segregated supramolecular columnar or spherical units. Of the columnar structures, most arrange in a hexagonal columnar *p6mm* symmetry 2D lattices. By far the most common spherical unit formation is the cubic *pm3m* symmetry lattice, although other arrangements, including body-centred cubic[13] and even quasi-crystalline[14] have been found. Surveys of dendron libraries reveal mesophase architecture to be less sensitive to the chemical nature of the molecular components than to the shape that the branching imposes. Specifically, molecular taper angle, as well as its projected solid angle, have been observed as primary determinants of self-assembly structure.[15] Control over these parameters has been achieved *via* a choice of branching level,[16] branching pattern,[17] dendron generation number,[18,19] branching groups,[20] apex group volume[21] and temperature.[22] For example, the dendron with a mono-substituted external benzyl ether in Fig. 1a, exhibits a planar tapered shape, allowing coassembly into columns that self-organise hexagonally. However, its tri-substituted analogue (Fig. 1b), favours a more conical shape, directing the coassembly into spherical objects, that in turn self-organise on a cubic lattice. Aside from structural considerations, enhancing mesogenic phase stability has also been a key objective in the rational synthesis of dendron species. This has been achieved by changing apex group H-bonding,[23] by ionic complexation between *endo*-receptor apex group and suitable salt,[24] or by substitution of alkyl groups for more rigid semi-fluorinated groups in the periphery regions.[25] All these factors influence stability through the modulation of micro-segregated domain miscibility. A recent review by Percec and coworkers showcase the synthesis, characterisation, and *meso*-structural control of these highly fascinating species.[26]

The fact that seemingly generic molecular traits govern dendron phase structure, suggest these compounds as highly suitable for coarse-graining molecular simulation studies. Here, by mapping distinct chemical groups onto "super-atoms", so to reduce the system dimensionality, one can partially resolve the timescale and system size requirements associated with mesophases that hamper all-atom simulation approaches.[28] Many procedures exist for assigning potentials to mapped sites, including angle-averaging all-atom potentials,[29] matching to structural properties,[30] obtaining them from equations of state[31] or force matching between groups of atoms.[32] A full review of coarse-graining methods would be out of place here, however the reader is referred to some excellent reviews on the topic.[33,34] In this paper we report the global fluid phase behaviour of a model coarse-grained dendron species. Here we use a more heuristic approach to assigning CG potentials, building in chemical detail with a minimum number of parameters to match rough molecular association, size and flexibility properties. Since our main interest was to achieve a topological map of phase transitions between observed and possibly unseen phases for a generic dendron model, we are content to compromise the quantitative gains that could be achieved by a more rigorous coarse-graining

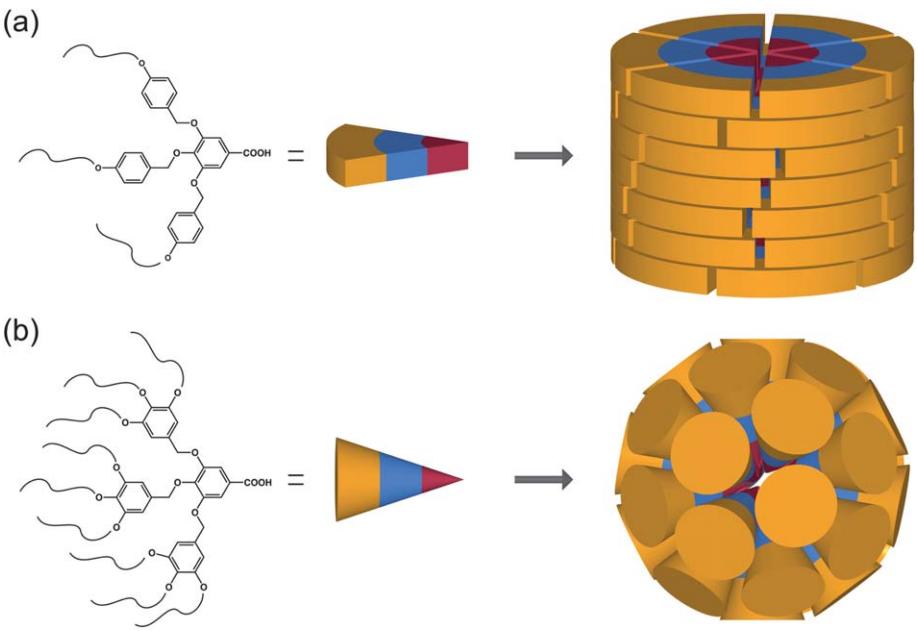

Fig. 1 Examples of dendritic tapered molecules and their reported self-assembly (a) 3,4,5-tris(4-alkyl-1-oxy)benzyloxybenzoate a mono-substituted flat tapered shaped dendron that self-assemble into hexagonal columnar mesophases (b) 3,4,5-tris[3,4,5-tris(alky-1-oxy)-benzyloxy]benzoate a tri-substituted conical shaped dendron that coassembles in spherical supramolecular units, that further self-organise into a cubic pm3m symmetry lattice. Adapted from ref. 27.

of a specific dendron molecule. This approach has successfully been applied to other liquid crystalline systems, including shape-persistent macrocycles,[35,36] end-tethered nanorods,[37,38] bolaamphiphiles with lateral chains,[39–41] banana-shaped mesogens[42] and star-polyphilic mesogens.[43] Following on, we describe our dendron model, before reviewing its observed phases, as well as an interesting unreported supramolecular sphere fluid mesogenic phase.

2 Molecular model

A simple coarse-grained model of a flat tapered dendron is implemented. In the model, four beads in a rigid planar diamond configuration form a central unit, defined by a perimeter 1.26σ bead separation and an acute internal angle of 60°. Here σ is a characteristic length of the model, identified as roughly the diameter of a bead. Grafted to each diamond are a single one-bead chain, bonded to a bead at the non-acute diamond vertex, and three two-bead chains, bonded to the remaining diamond beads. The resulting topology is depicted in Fig. 2a. To model semi-flexibility into the grafted chains, harmonic angular and bond length potentials are used,

$$U_{\text{bond}} = \frac{1}{2}k_{\text{bond}}(r - r_{\text{o}})^2 \tag{1}$$

and

$$U_{\text{ang}} = \frac{1}{2}k_{\text{ang}}(\theta - \theta_{\text{o}})^2 \tag{2}$$

with r and θ being the bead separation and angle between adjacent bonds, r_{o} and θ_{o} the equilibrium bead separation and bond angles, and k_{bond} and k_{ang} the bond and angular spring constants. In the model an equilibrium distance of $r_{\text{o}} = \sigma$ and spring constant of $k_{\text{bond}} = 50\varepsilon\sigma^{-2}$ are used for all non-rigid bonds. For the angular potentials an equilibrium angle of π rad and spring constant of $k_{\text{ang}} = 50\varepsilon\text{rad}^{-2}$, are used throughout. The bead bond vectors used to define these angular harmonic potentials are given in Fig. 2a. The overall choice of bonding potentials and rigid constraints imposed on the core of the dendron a planar tapered shape. The rigid core rigid unit is used to uniquely specify an orientation of each molecule with respect to a fixed coordinate frame, assigning coordinate axes to each dendron. Finding the distribution of molecular orientations is useful in defining structural order parameters, as will be explained later. Our chosen rigid body coordinate frame is indicated in Fig. 2b.

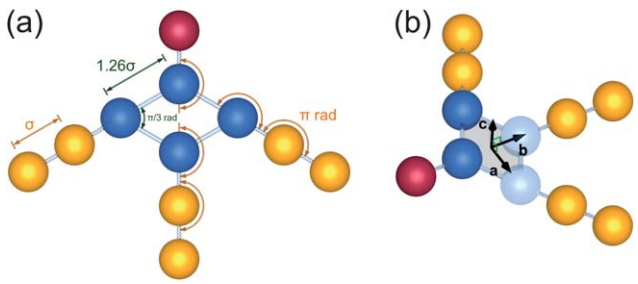

Fig. 2 Schematic of model dendron showing (a) the model geometry and (b) the internal axes assigned to the rigid-unit axes. Here type 1 beads are coloured red, type 2 beads are coloured blue and type 3 beads are coloured yellow. This colour scheme is used throughout the paper.

To discern the three regions of a typical dendron we define three bead types into our model. Type 1 beads, located at the tapered-tip (color coded red in the figures) are defined with self-attraction between themselves, so as to represent a generic associating apex group, such as a hydrogen bonding moiety. Type 2 beads (color coded blue), located in the rigid diamond unit are also defined to have a weak self-attraction, to mimic π–π interactions that may occur between dendritic benzyl ether groups. Type 3 beads (color coded yellow), form the three two-bead grafted chains, are defined to be mutually repulsive, to mirror the weaker interactions found between alkyl chain periphery groups. Finally, and importantly, all bead cross-interactions are set as soft repulsive, so to confer an inherent immiscibility between bead types, analogous to that found in real polyphilic dendrons. In the spirit of simplicity, all six bead pair potentials are defined through the Lennard-Jones cut and shifted potential, $U_{\text{AB}}^{\text{LJCS}}$, given by

$$U_{\text{AB}}^{\text{LJCS}}(r; C_{\text{ij}}) = \begin{cases} U_{\text{AB}}^{\text{LJ}}(r) - U_{\text{AB}}^{\text{LJ}}(C_{\text{AB}}) & \text{for } r < C_{\text{AB}} \\ 0 & \text{for } r \geq C_{\text{AB}} \end{cases} \tag{3}$$

with

$$U_{\text{AB}}^{\text{LJ}}(r) = 4\varepsilon_{\text{AB}}\left[\left(\frac{\sigma_{\text{AB}}}{r}\right)^{12} - \left(\frac{\sigma_{\text{AB}}}{r}\right)^{6}\right] \tag{4}$$

where the subscripts A and B define bead type, r is the bead separation, ε_{AB} an energy parameter defining the potential well depth, σ_{AB} a length parameter that defines the potential range, and C_{AB} is the cut and shift distance. The parameters used for each pair potential are summarised in Table 1. Here, all bead pairwise interactions have the same σ_{AB}, set equal to σ, our characteristic length. The C_{AB} of $2^{1/6}\sigma$ is used for all cross-interactions and type 3 bead self-interactions and corresponds to a cut and shift at the minimum of the Lennard-Jones potential, and thus maps into a soft-repulsive WCA fluid.[44] Overall, the approach here is similar to strategies used in modern equations of state, such as SAFT, where one describes a fluid by a hard core reference system, and includes attractive interactions arising from dispersion interactions, electrostatics, or possibly hydrogen bonding as perturbations which are sequentially added.[45,46]

The temperature, $T^* = Tk_b/\varepsilon$, where k_b is Boltzmann's constant, pressure, $P^* = P\sigma^3/\varepsilon$, and time $t^* = t/(m\sigma^2/\varepsilon)^{1/2}$, are expressed throughout this work in the standard reduced form that reflects the energy (ε) and length (σ) scales of the model.

3 Phase characterisation

The structured mesogenic phases observed during the course of the simulations are monitored through the computation of order

Table 1 Table defining force field LJCS parameters used for each non-bonded pair, listed as (ε_{AB}, C_{AB}); all spheres sizes are equal $\sigma_{\text{AB}} = \sigma$

	Type 1	Type 2	Type 3
Type 1	ε, 2σ	ε, $2^{1/6}\sigma$	ε, $2^{1/6}\sigma$
Type 2	ε, $2^{1/6}\sigma$	$5\varepsilon/6$, 2σ	ε, $2^{1/6}\sigma$
Type 3	ε, $2^{1/6}\sigma$	ε, $2^{1/6}\sigma$	ε, $2^{1/6}\sigma$

parameters. These allowed a quantitative understanding of the phases to be achieved and help locate phase transitions. A brief overview of these is provided.

3.1. Orientational order parameters

A columnar order parameter, S_2, is defined as

$$S_2 = \frac{\sum_{j=1}^{N}\left(3sin^2\phi_j - 1\right)}{2N} \quad (5)$$

with ϕ_j the angle between a self-assembled columnar axis (if it exists) and the j^{th} dendrons' b-axis, as defined in Fig. 2b. The system's columnar axis is also defined in terms of these b-axes, taken as the vector maximally orthogonal to them. The general procedure has been outlined previously.[39] For an isotropic system the columnar axes and individual dendron b-axes are uncorrelated, and S_2 takes a value close to 0. Conversely with columnar ordering, most ϕ_j are close to 90°, and S_2 tends to 1. This order parameter monotonically changes between these extremes, and consequently provides a good metric of columnar ordering.

Orientational ordering of dendron c-axes is studied by monitoring the standard nematic order parameter, P_2, defined as

$$P_2 = \frac{\sum_{j=1}^{N}\left(3cos^2\theta_j - 1\right)}{2N} \quad (6)$$

with θ_j the angle between the c-axes defined director and the j^{th} dendrons' c-axis, as defined in Fig. 2b. As with S_2, a nematic order parameter of 1 indicates complete orientational order, and that of 0 indicates absence of order. For columnar structures, S_2 and P_2, provided complementary information on rotational dendron motion about the c-axes.

3.2. Cluster analysis

Many of the mesogenic phases associated with our model dendron were found to involve supramolecular spherical structures with type 1 beads grouped in their centre. To quantitatively study this phenomena we perform cluster analyses on these meso-structures. Here type 1 beads were defined to be in the same cluster if located within a 1.5σ cut-off separation of one another, and/or if connected by a path of clustered type 1 pairs. From this, a discrete distribution, $D(i)$, of cluster sizes, i, was obtained, that could in turn be used to determine individual order parameters associated with clustering. For example, the average size of clusters, n_{ACS}, given by

$$n_{ACS} = \sum_{i=1}^{\text{Largest Cluster Size}} i \times iD(i)/N \quad (7)$$

provide a measure of supramolecular sphere sizes in the system, whilst the fraction of monomers, f_{mon}, given by

$$f_{mon} = D(1)/N \quad (8)$$

provides a measure of clustering levels in the system as a whole. Finally, the distribution of cluster sizes, $F(i)$, for cluster size i, given by

$$F(i) = iD(i)/N \quad (9)$$

provides a measure of the spread of cluster sizes.

Clusters in the system above a certain size could themselves be treated as supramolecular spheres, thus permitting structural analysis on length scales beyond individual dendrons. These supramolecular spheres were characterized by the position of centre of mass of the type 1 beads within each cluster. Based on these supramolecular sphere positions it was possible to investigate either fluid structural behaviour by studying their radial distribution functions, *rdf*, or crystalline structural order by looking at their Steinhardt type order parameters.[47,48] The Steinhardt type order parameters, q_l, used in this study are defined by

$$q_l = \sqrt{\frac{4\pi}{2l+1}\sum_{m=-l}^{m=l}\left|\frac{\sum_{i=1}^{N_{cluster}}\sum_{j=1}^{N_b(i)} Y_{lm}(\mathbf{r}_{ij})}{\sum_{i=1}^{N_{cluster}} N_b(i)}\right|^2} \quad (10)$$

with $\mathbf{r}_{ij}$ the vector between the i^{th} and j^{th} cluster positions, $N_{cluster}$ the total number of clusters over the threshold size, $N_b(i)$ the number of clusters within a threshold distance of cluster i, and $Y_{lm}(\mathbf{r}_{ij})$ the spherical harmonic for the polar coordinates of $\mathbf{r}_{ij}$ in an arbitrary coordinate system. With even-l spherical harmonics, the ensuing q_ls are invariant to chosen coordinate frame, and by looking at their ratio of values provide evidence of crystal structure type. The choice of nearest neighbour separation cut-off for the clusters was decided by reviewing the cluster *rdf* of both lattice and fluid supramolecular sphere structures, and taken as a constant of 12.5σ. As the cluster *rdf* peak positions remained relatively constant over different *PT* state points a constant cut-off was deemed adequate. The minimum size of clusters included in the analysis was 11 dendrons, and the analysis was only performed for configurations with a total cluster count greater than 30, for our 2000 dendron simulations. As to be shown, these values were guided by the cluster size distribution, $F(i)$, found at different state points.

4 Simulation details

All simulations were performed in continuum space *via* molecular dynamics with the DL_POLY simulation suite.[49] The extended-Lagrangian approach was used to simulate either the isotension-isothermal *NsT* ensemble or the isobaric-isothermal *NPT* ensemble, the former being implemented for simulations containing non-isotropic fluid phases. All simulations were performed with a timestep of $\Delta t^* = 0.0125$, with periodic boundary conditions, and with 2,000 dendron molecules.

To explore different aspects of the model dendron phase behaviour a number of distinct simulations were performed, as outlined below.

4.1. Qualitative phase diagram survey simulations

To examine the global phase behaviour, over 1000 simulations were performed along various isotherms and isobars. Here, equilibrated or partially equilibrated configurations from one state point were used as inputs for adjacent state points in the

series, then run with variable length equilibration and data collection periods. A typical equilibration period of 200,000 steps was used, though shorter equilibration runs, down to 50,000 steps, were used for fully isotropic states, and longer equilibration runs, up to 2,000,000 steps, were used for states close to expected phase transitions. Ultimately the length of these simulations was dictated by a requirement that output configurations appeared fully equilibrated and suitable for a data collection. Data collection simulations were typically run for 1,000,000 steps with configuration sampling performed over intervals of 10,000 steps. Though not entirely systematic, broadly speaking most of the computational resources were expended on the structured mesogenic phase regions of most interest.

4.2. Self assembly simulations

Temperature quench simulations were performed to demonstrate self-assembly of observed mesogenic phases from initially isotropic and homogeneous states.[50] These simulations were performed until an equilibrium phase was achieved, as indicated by order parameter monitoring. Data sampling was performed at varying time intervals during these simulations, guided by the timescales associated with the various stages of self-assembly observed. These simulations were an independent check of phase stability.

5 Results and discussion

The model dendron global phase diagram in Fig. 3 was mapped by performing simulations over a range of temperatures and pressures. Here, each of the four observed phases are shown; a hexagonal columnar (HC) mesogenic phase, a supramolecular sphere body-centred cubic (SSbcc) mesogenic phase, a supramolecular sphere fluid (SSf) mesogenic phase and a fully isotropic phase. For clarity the results are first presented for a temperature variation along a single isobar, describing the mesogenic phases, their structural character, transitions, and relative placing within the global phase diagram. Following that, a description of supramolecular self-assembly mechanisms is given.

5.1. Global phase diagram

Temperature variation simulation results for the model dendron along the $P^* = 0.157$ isobar are presented in Fig. 4, and reviewed from low to high temperature. As seen in Fig. 3, this isobar traverses the domains of all observed phases. We use this path to fully describe the different phases encountered.

5.1.1. Hexagonal columnar mesogenic phase. The lowest temperature phase along the isobar is the hexagonal columnar mesogenic phase. Here model dendrons coassembled into columns, with type 1 beads micro-segregated in the column centre and type 3 beads in the column periphery. These columns in turn self-organised into a hexagonal arrangement. In the columns the dendrons orient such that their b-axes are orthogonal to the columnar axes, giving rise to a high columnar order parameter, S_2. Moreover the dendron c-axes nematic order parameter, P_2, is also high, indicating their orientational order, and hence low rotational motion about their b-axes. Whilst a quantitative dendron self-diffusion study was not performed, visual analysis of simulation movies provided satisfactory evidence of dendron mobility within the supramolecular columns. By isolating individual dendrons in the movies (not

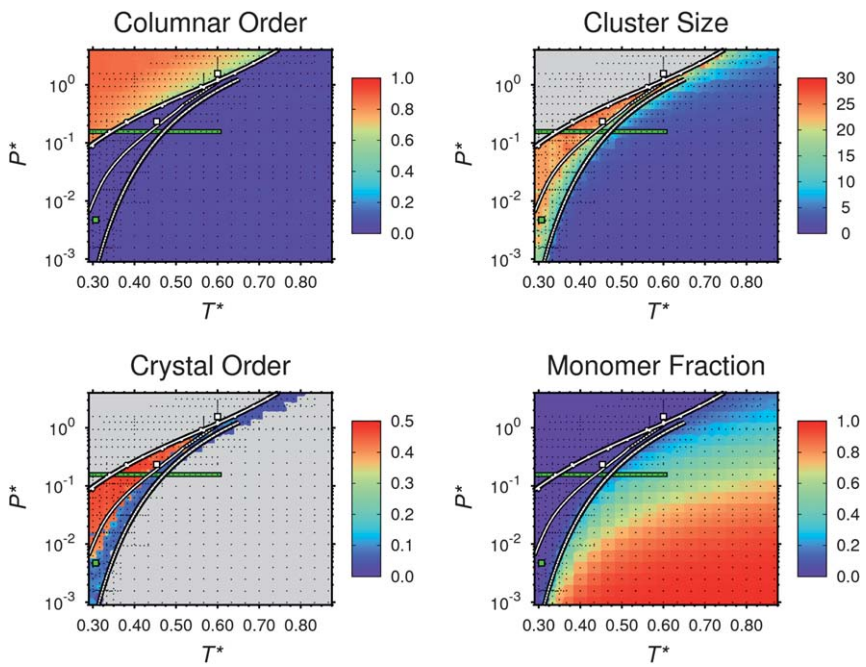

Fig. 3 Contour plot of *PT* phase diagrams displaying (a) Columnar order parameter, S_2 (b) Average cluster size, n_{ACS} (c) The 6th order Steinhardt order parameter for aggregate clusters, q_6 (d) Dendron monomer fraction, f_{mon}. Phase transitions are shown as white in black lines. Also shown are the *PT* points of the self-assembly simulations (white in black squares), of the SSf phase of Fig. 7 (green in black square), and the isobar presented in Fig. 4 (green in black line). Small black points represent each simulated state point.

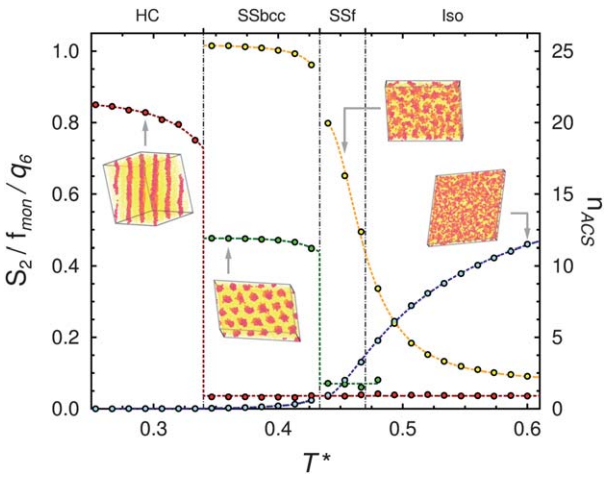

Fig. 4 Plot of order parameters as a function of temperature, T^*, at $P^* = 0.167$. The columnar order parameter, S_2 (red line), 6th order Steinhardt order parameter for supramolecular spheres, q_6 (green line), average cluster size, n_{ACS} (yellow line) and monomer fraction, f_{mon} (blue line) are shown. Phase transitions between the labelled phases are delineated by vertical grey lines. Snapshots are representative state configurations for each mesophase; only type 1 and 3 beads are drawn for clarity.

included) it is possible to see diffusion of dendrons both around the columns and up and down the columns. This provides clear evidence of the phase's mesogenic character. As the monomer fraction, f_{mon},. was near zero for this columnar phase, the dendron, though mobile, were still confined to the column. Since the average dendron cluster size occupancy, n_{ACS}, is ill defined for the columnar phase, it was omitted from the order parameter plot of Fig. 4.

At higher pressures and lower temperatures the HC mesogenic phase is dominant, clearly visible in the S_2 colour map of Fig. 3a. To produce the global phase diagram, discontinuities in S_2 are used to locate transitions from the columnar phases, that are then used to fit coexistence curves. At higher pressures this phase undergoes a first-order transition to the SSf phase upon an increase in temperature. This is seen in Fig. 3b and 3d, respectively, with n_{ACS} changing to between 15 and 25, and q_6 near zero, at temperatures above this coexistence curve. At lower pressures, the HC phase has a first-order transition into the SSbcc phase with increasing temperature, as seen by the n_{ACS} between 20 and 25, and q_6 of between 0.45 and 0.50. As isotherm simulation across these transitions were typically run with increasing temperatures along the series, hysteresis may have shifted these transitions to slightly higher temperatures.

As alluded to in the introduction, HC mesogenic phases, are commonly observed for flat tapered dendron species. This behaviour was straightforwardly captured by our model. Simulations at the lowest temperatures and highest pressures reported in Fig. 3 correspond to a glassy solid HC phase with slowly growing region of crystallinity. Here, both S_2 and P_2 continue to increase with decreasing temperature, though with visibly increasing roughness, that could be attributed to erratic annealing. In consequence, transition from the mesogenic HC phase to a possible crystalline HC phase is hard to locate, though most likely exists. Crystalline HC phases have been seen experimentally.[26]

5.1.2. Supramolecular body-centred cubic lattice mesogenic phase. Upon increasing temperature along the isobar, a transition at $T^* = 0.340$ occurs from the HC mesogenic phase to the SSbcc mesogenic phase. Here model dendrons coassemble into spherical supramolecular spheres, such that type 1 beads are micro-segregated in the sphere centre and type 3 beads are relegated to the sphere periphery. These supramolecular spheres self-organise onto a body-centred cubic (bcc) lattice. The ensuing lack of global dendron orientational order results in a drop in S_2 and P_2 to near zero, and clearly delineates the transition from the columnar phase. A value of n_{ACS} around 25 provides a measure of the size of the supramolecular spheres, and the value of q_6 around 0.5 confirms the visual observation of supramolecular order. Though not reported in Fig. 4, the remaining Steinhardt order parameters are consistent with a bcc structure. Isolated individual dendrons diffuse internally within individual supramolecular spheres, and on a longer time scale diffuse between supramolecular spheres. This, along with the fluidity required for self-assembly, provides ample evidence of the mesogenic nature of the phase.

Further information about this phase can be gathered from the supramolecular sphere *rdf* and $F(i)$ distribution of a simulation performed at $T^* = 0.317$ and $P^* = 3.31 \times 10^{-2}$, shown in Fig. 5 and 6, respectively. In Fig. 5, the *rdf* peaks of an ideal bcc lattice of commensurate length – though with peaks scaled down for clarity – further supports the bcc structural interpretation. The peak's relative sharpness also supports the observation of supramolecular sphere pseudo-crystalline organisation. This *rdf* was used to justify the choice of a 12.5σ nearest neighbour cut-off used for the calculation of the Steinhardt order parameters of the structure. With this cut-off length the two nearest neighbour types found are illustrated in Fig. 5. The $F(i)$ distribution in Fig. 6, shows the narrow distribution of aggregate sizes typically found, and justifies the treatment of the supramolecular spheres

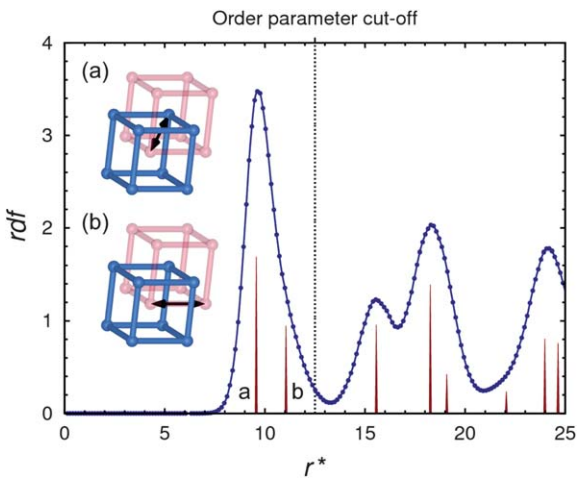

Fig. 5 Cluster radial distribution function, *rdf*, averaged over configurations from the SSbcc phase self-assembly simulation at $T^* = 0.317$ and $P^* = 3.31 \times 10^{-2}$ (blue line), *cf.* the Fig. 13b "final states", and ideal bcc structure *rdf* peaks (red lines). Here ideal crystal peaks are proportionally sized though reduced in scale for clarity. Peaks (a) and (b) correspond to the two types of nearest neighbours included with the 12.5σ choice of cut-off used for the determination of the Steinhardt order parameters.

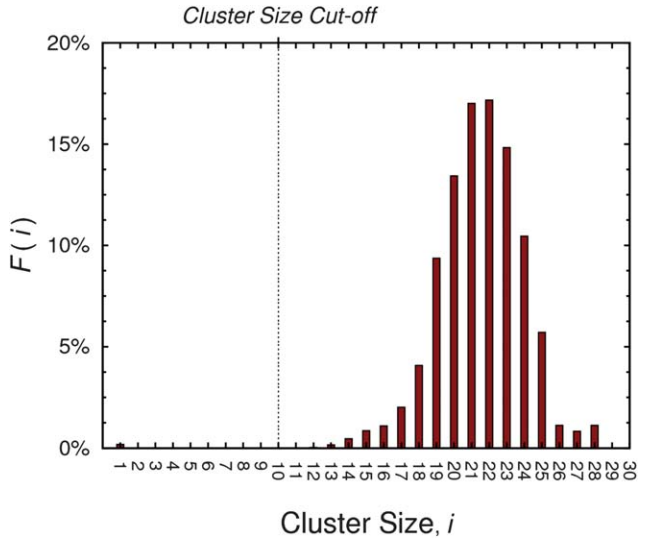

Fig. 6 Cluster size distribution, $F(i)$, for the SSbcc phase at $T^* = 0.317$ and $P^* = 3.31 \times 10^{-2}$.

as distinct entities. This distribution was used to decide the minimum size clusters to include in the cluster analysis.

For actual dendron systems, supramolecular spherical structures are typically observed for dendrons with a conical shape. Since we impose a planar tapered shape in our model, the transformation from the columnar phase is in part attributed to the rotational motion about the b-axes creating an effective conical profile. As will be described later, this was borne out by the fact that supramolecular spherical mesogenic phases are stable at lower pressures, permitting the larger molecular volume required for rotational diffusion. The fact that our model self-assembles into spherical entities is a unique and unexpected feature of our study. It is however, one of the most salient conclusions, as it proves that not only is the overall shape of the molecule the determinant factor in its self-organization, but also the thermodynamic conditions play a decisive role. As most experiments are performed in a very narrow range of pressures and temperatures, these effects have presumably been overlooked.

5.1.3. Supramolecular sphere fluid mesogenic phase. With increasing temperature a pseudo solid-fluid transition occurred at $T^* = 0.433$, with the supramolecular lattice melting into the SSf mesogenic phase. Though n_{ACS} stays high for this phase, showing the persistence of supramolecular spheres, a drop in q_6 to near zero demonstrates that there is no positional ordering, hence they have a fluid like structure.

Further information about this phase is summarised in Fig. 7, for a simulation configuration taken at $T^* = 0.301$ and $P^* = 4.67 \times 10^{-3}$. Snapshots of the simulation and mapped supramolecular sphere positions, in Fig. 7a and b, suggest a liquid-like form. This is confirmed by calculation of the supramolecular spheres *rdf*, shown in Fig. 7d, whose broad peaks are characteristic of a dense fluid. For the SSf mesogenic phase the narrow peak in the cluster size distribution, $F(i)$, shown in Fig. 7c, again substantiates treatment of the aggregated dendrons as supramolecular units.

The SSbcc mesogenic phase is stable at higher temperatures and lower pressures than the HC mesogenic phase, as is evident in the n_{ACS} and q_6, plots of Fig. 3b and d, respectively. With increasing temperature this phase experiences a first-order phase transition into the SSf phase, seen in Fig.3d by the drop in q_6. In contrast to using this discontinuity of q_6 along isotherms and isobaric simulations to estimate the SSbcc-SSf coexistence curve – that would be influenced by hysteresis – free energy methods were used. Here, by introducing an external field that coupled to type 1 bead positions on a bcc lattice, it was possible to obtain a quasi-static path from the SSbcc to SSf phase that bypassed the first-order transition. This allowed relative Gibbs free energies of the states in both phases to be found by thermodynamic integration, and hence to determine a coexistence point, by equality of the phase's Gibbs free energy. The Gibbs–Duhem method – using simulation coexistence point data of both phases – was performed to iteratively solve the Clapeyron equation, tracing the coexistence curve out from the previously determined coexistence point.[51,52] The resulting coexistence curve is presented in Fig. 3. More details on the method used may be found elsewhere.[53]

The SSf mesogenic phase is located at temperatures between the HC or SSbcc mesogenic phases and the isotropic phase, seen clearest in the q_6 plot of Fig. 3d. With increasing temperature the supramolecular dendrimer fluid undergoes a continuous transition to the isotropic phase. The strength of this transition was found to decrease with increasing temperature and pressure, as shown in Fig. 9. For higher temperatures and pressures it became unfeasible to determine the position of this transition, so the fitted transition curve is given up to this point only. In this region, from inspection of simulation movies, diffusion of dendrons between clustered aggregates appears more rapid, hence treatment of the aggregates as supramolecular units is more tenuous.

At lower pressures in the SSf mesogen phase domain, the density of supramolecular spheres is found to decrease, passing from a more liquid-like to gas-like unstructured behaviour. Whilst we looked for a pseudo gas-liquid transition for the SSf phase, it was not seen. As the outer type 3 beads of the supramolecular structures are fully repulsive, it may be expected that the effective supramolecular units potential is also repulsive. In this case, one would not expect a pseudo gas-liquid transition, as attractive interactions are a requisite for this phenomena. Using the sphere *rdf* of a state point in the supramolecular sphere fluid phase domain, an iterative Boltzmann inversion[54–57] could be performed to determine the single[58,59] effective spherical sphere pair potential that maps to the *rdf*. As an aside, one could also extend these calculations over a range of state points to study the variation of such an effective potential, in a sense going up a level in the coarse-graining hierarchy.

We note that although this phase is reminiscent of a micellar structure, there are two fundamental differences. Firstly, we do not consider solvents; our systems are pure fluids. Secondly, the distribution of dendrons per sphere is very sharp; the pseudo spheres are all roughly the same size. Whilst the HC and SSbcc mesogenic phases have been observed experimentally in dendrons, the SSf phase to the best of our knowledge, has not been reported, and as such is a prediction of our model. Since there is a continuous transition separating it from the isotropic phase (see below), its identification as distinct from the isotropic phase is hindered.

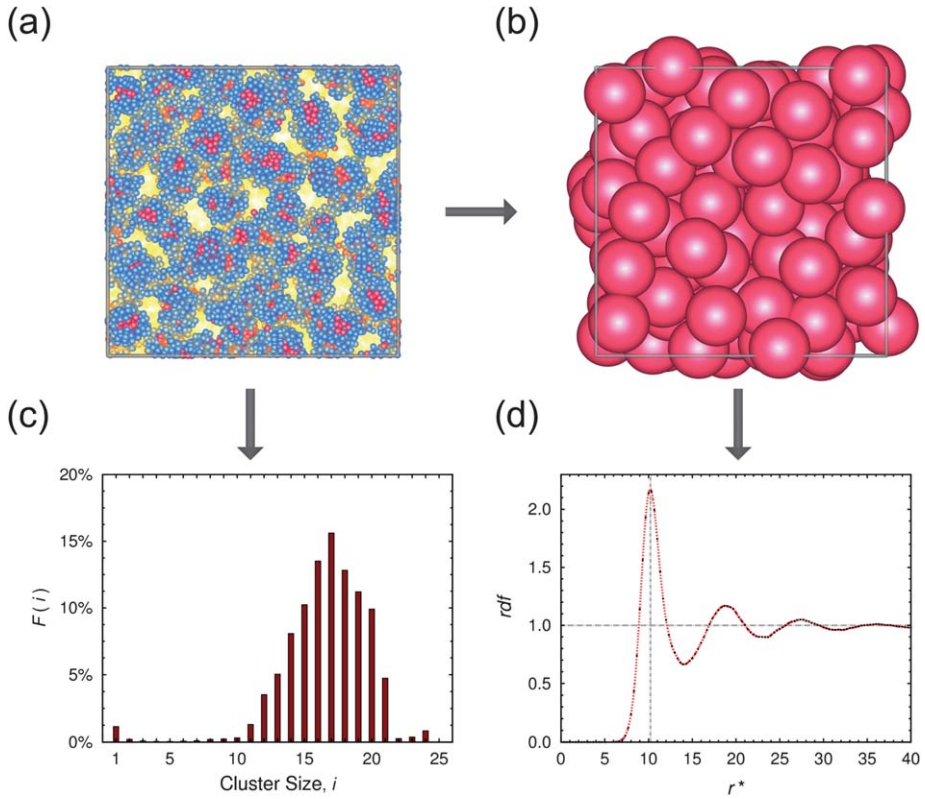

Fig. 7 Diagram of the SSf phase at $T^* = 0.301$ and $P^* = 4.67 \times 10^{-3}$, showing (a) A simulation configuration snapshot, (b) the supramolecular sphere positions of the same configuration, (c) the cluster sizes distribution, $F(i)$, and (d) the supramolecular sphere *rdf*. The two plots were generated from a larger simulation of 16,000 dendrons, to allow the first three shells of the *rdf* to be captured.

5.1.4. Isotropic phase. With a further temperature increase the SSf mesogenic phase undergoes a continuous transition to the isotropic phase, characterised by high monomer fraction and no dendron orientational order. Whilst this transition is evident from changes in n_{ACS} or f_{mon} (*cf.* Fig. 4), another source of information is the cluster size distribution, $F(i)$, of Fig. 8. This shows the mean cluster size decreasing with increasing temperature, with the cluster peak getting smaller whilst merging into a growing monomer peak. To assign an approximate temperature to this transition, the peak of $(\partial f_{mon}/\partial T)_P$ from fitted isobaric $f_{mon}(T)$ curve is used. This choice is justified at lower pressures by the steeper continuous transitions found, as shown in Fig. 9. It should be pointed out that we have no supporting

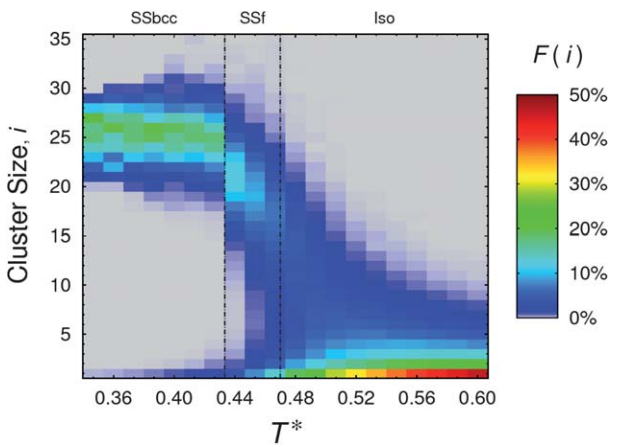

Fig. 8 Contour plot of cluster sizes distribution, $F(i)$, as a function of temperature at $P^* = 0.157$.

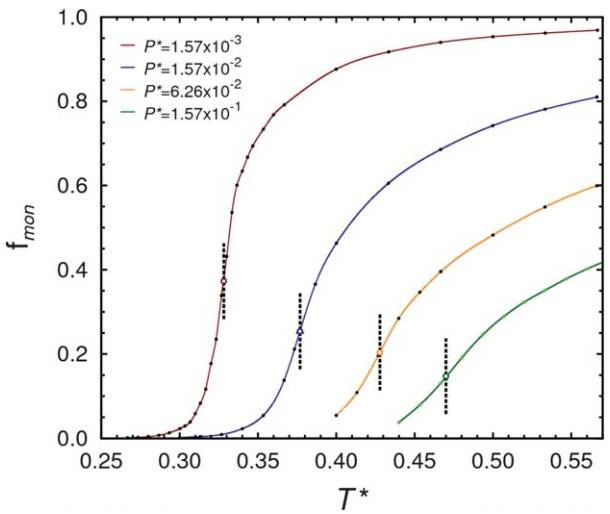

Fig. 9 Plot of dendron monomer fraction, f_{mon}, as a function of temperature for four isobars in the vicinity of the SSf to isotropic phase transition. The transition temperatures (black dashed bars) were assigned as the steepest parts of the curves, and found from the peak of the derivative of a fitted f_{mon} with respect to temperature.

evidence for this to be a actual phase transition, as opposed to a chemical equilibrium between monomers and the spherical mono-disperse spherical entities.

5.2. Self-assembly

On performing simulation series along isobars or isotherms, there exists a risk of stable structured phases templating the formation of metastable structured phase at other state points. For example, when passing from the SSf to SSbcc phase the n_{ACS} differed from that found at the same state point by approach from the SSbcc phase. This hysteresis is presumably an artefact of the molecular dynamics approach used. To pass from one equilibrium n_{ACS} to a higher one, at another state point, a fraction of supramolecular spheres would have to be destroyed and their dendrons redistributed among the remaining spheres. Conversely, going from higher to lower n_{ACS} requires each supramolecular sphere to shed some dendrons to create new spheres. In either case, the destruction or creation of supramolecular spheres creates defects in the lattice, and requires a lattice rearrangement to remove this and reach equilibrium. The time scales for diffusion of molecules required for supramolecular sphere generation/destruction, along with supramolecular sphere lattice rearrangement, are prohibitively long even for these coarse-grained simulations.

To corroborate that the observed structured fluid phases were actual equilibrium states and to monitor the dynamics of the self-assembly process, two relatively long simulations were performed, initiated from configurations with no structural order. The simulation points are highlighted in Fig. 3. As these are coarse-grained models, the diffusion process is expected to be at least an order of magnitude faster than the corresponding real process,[40] however, the relative timescales of the different phenomena are expected to be correct. This is a fortuite aspect of the coarse-graining process, of which we take advantage herein.

5.2.1. Hexagonal columnar mesogenic phase. A self-assembly simulation of the HC mesogenic phase was performed by quenching to a state at $T^* = 0.633$ and $P^* = 3.13$. Representative snapshots of configurations from this simulation, along with the temporal variation of S_2, and f_{mon} are presented in Fig. 10 and 11, respectively. As seen in Fig. 10a the simulation was initiated from a homogeneous and isotropic initial non-equilibrium state. Here f_{mon} started at around 0.17, and S_2 close to zero. The first stage of self-assembly was marked by a rapid clustering of dendrons into aggregate structures with type 1 beads grouping together. This clustering was followed by an exponential decay of f_{mon}, seen in the inset of Fig. 11, essentially complete after $t^* = 2000$, with ensuing aggregate structures shown in Fig. 10b. The second stage of self-assembly involved aggregate coalescence into larger clusters that in turn self-organise into a hexagonal columnar arrangement. An intermediate stage in this process is given in Fig. 10c. During this period f_{mon} slowly decreased in a more linear fashion, whilst S_2 increased. This increase is partially attributed to the increased columnar order, as well as growth of a dominant columnar domain at the expense of the depletion of smaller ones. The final equilibrium structure of the HC mesogenic phase is presented in Fig. 10d, and is achieved at a time of $t^* = 120{,}000$, a time two orders of magnitude larger than the time needed for the initial clustering stage. The hexagonal columnar arrangement and micro-segregation of bead types are clearly shown in the cross-section slice of Fig.10d.

5.2.2. Supramolecular bcc lattice mesogenic phase. A self-assembly simulation of the SSbcc mesogenic phase was performed at $T^* = 0.317$ and $P^* = 3.31 \times 10^{-2}$. To describe the time evolution of the self-assembly process the f_{mon}, n_{ACS}, and q_l order parameters were monitored, as presented in Fig. 12, along with representative simulation snapshots, examples given in Fig. 13. As with the HC mesogenic phase, multiple stages of self-assembly occurred over different time and length scales. The input non-equilibrium homogeneous and isotropic state, shown in Fig. 13a, was initially found to undergo rapid dendron coassembly with type 1 beads clustering together. In Fig. 12, this period was tracked by a drop of f_{mon} from roughly 0.4 to near zero, and by increasing n_{ACS} from around 4 to 22, within $t^* =$ 10,000. In contrast to the HC phase, the initially formed aggregates are stable supramolecular units at this state point, and did not merge into larger structures. After $t^* = 10{,}000$ it was therefore possible to treat them as supramolecular particles, and study their Steinhardt order parameters to follow the supramolecular organisation. Between $t^* = 10{,}000$–$70{,}000$ the supramolecular spheres were confined in an amorphous state, as seen in Fig. 13b. During this period each of the q_l's were close to zero, and increased only modestly, as seen in Fig. 12b. At $t^* = 70{,}000$ a rare event pushed the supramolecular spheres into a lattice state. By comparison of the supramolecular sphere q_l's with perfect crystal q_l's, generated using the nearest neighbour types illustrated in Fig. 6, in addition to visual analysis following the route of Fig. 13, the supramolecular lattice is confirmed to be bcc. With continued simulation the supramolecular crystal structured relaxed further between $t^* = 110{,}000$ and $t^* = 120{,}000$, with the q_l remaining constant after this stage. The trough in q_{10} and peak of q_4, suggested this relaxation between bcc structures involved passing through a face-centred cubic structure. Initial self-assembly to the correct architecture, as well as subsequent transition through another lattice to attain a defect free bcc lattice, were strongly indicative that the SSbcc mesogenic phase is an equilibrium one.

6 Perspective

We have studied the global fluid phase diagram of a coarse-grained model dendron by simulation. We imposed the geometry of a typical dendron by rigid constraints and bond-interactions, and the multiple domains of chemical composition by a judicious choice of non-bonding interactions. Our success in capturing both HC and SSbcc mesogenic phase, corroborates that dendron complex phase behaviour is more dependent on molecular shape anisotropy and relative domain immiscibility than on finer chemical structural features. This feature is a shared characteristic in other soft matter scenarios, *e.g.* lipid bilayer-forming amphiphiles[60] and self-assembly of DNA in lipids.[61] In essence, a broad domain of potential function space maps to mesogenic structured phases, permitting physical intuition to guide one to appropriate coarse-graining parameters in this region.

In addition to the experimentally reported structured supramolecular mesogenic phases, our model also exhibited the SSf

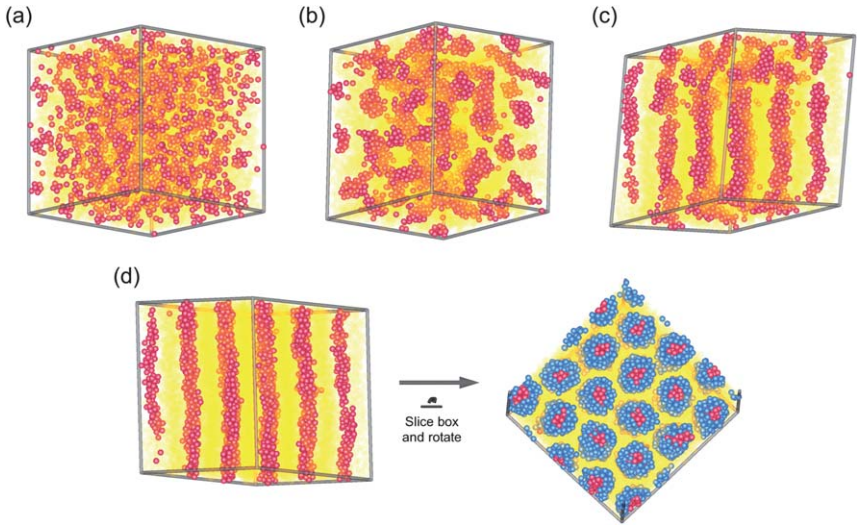

Fig. 10 Self-assembly of HC mesogenic phase at $T^* = 0.633$ and $P^* = 3.13$ from non-equilibrium isotropic and homogeneous state at (a) $t^* = 0$ (b) $t^* =$ 1,250 (c) $t^* = 75{,}000$ and (d) $t^* = 124{,}000$. For clarity only type 1 red beads and type 3 transparent yellow beads are indicated, except in the sliced snapshot of (d) where type 2 blue beads are also shown.

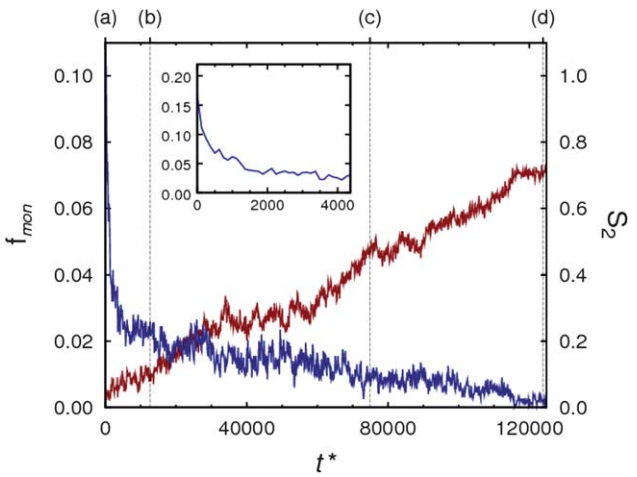

Fig. 11 Variation of monomer fraction, f_{mon}, and columnar order parameter, S_2, during HC phase self-assembly simulation at $T^* = 0.633$ and $P^* = 3.13$. Here f_{mon} and S_2 are given by the blue and red lines, respectively. The times of (a) to (d) corresponds to snapshots given in Fig. 10.

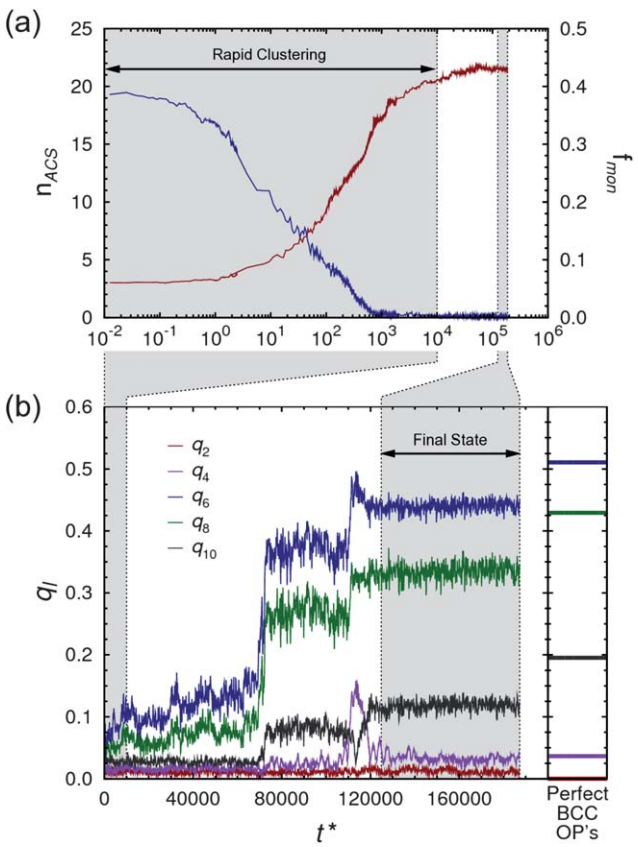

Fig. 12 (a) Variation of monomer fraction, f_{mon}, and average dendron cluster size occupancy, n_{ACS}, during SSbcc phase self-assembly, at $T^* = 0.317$ and $P^* = 3.31 \times 10^{-2}$. Here f_{mon} and n_{ACS} are given by the blue and red lines, respectively. (b) Variation of Steinhardt order parameters, q_l, during the same simulation.

phase, that to the best of our knowledge has been unseen in these molecules. In this phase a local structural order of dendrons in the supramolecular units is retained, but these objects have no long range correlation. At lower pressures this phase is clearly separated from the isotropic phase by a sharp continuous transition, at higher pressures this however weakens, and classification of the aggregates as supramolecular entities is more tenuous. Here a quantitative comparison of inter aggregate dendron diffusion against aggregate unit diffusion, could establish the timescales at which it is appropriate to label dendron clusters as supramolecular units. Experimental verification of such structures would in part depend on this timescale compared to X-ray (or similar) sampling times. Our work here suggests that experimental systems that undergo an indirect transition from the HC mesogenic phase to isotropic phase, *via* the SSbcc phase, are the best candidates for discovering a SSf phase. This is because the lower pressures that stabilise this intermediate phase, appear to

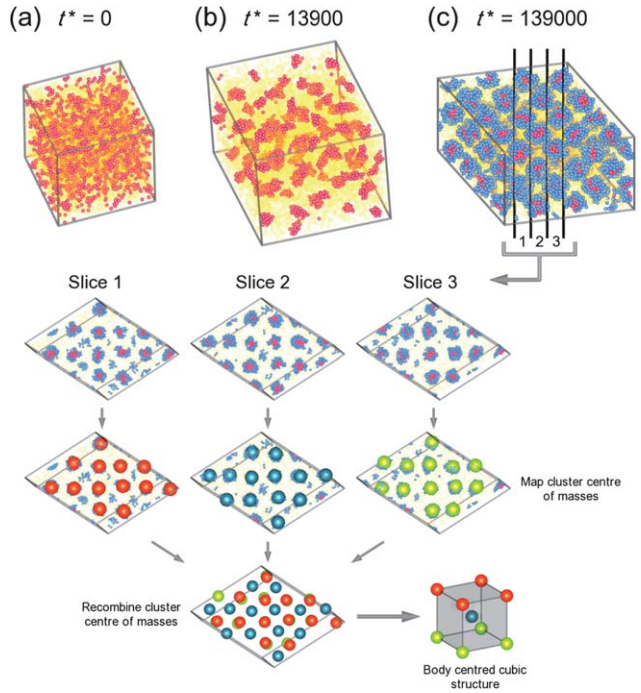

Fig. 13 Self-assembly of SSbcc structure at $T^* = 0.317$ and $P^* = 3.31 \times 10^{-2}$ from non-equilibrium isotropic and homogeneous state. For clarity only type 1 red beads and type 3 transparent yellow beads are indicated at times (a) and (b). The lower half of the diagram schematically illustrates the bcc structure of the final equilibrium phase.

stabilise supramolecular sphere lifetimes. Though the bcc lattice phase we observed has been seen in experiments,[13] they are far less commonly seen than the *pm3m* cubic symmetry lattice. If we presume that co-assembled dendrons behave as effective particles, with ensuing effective pair potentials, then we may say that our model produces the wrong effective potential to achieve pm3m cubic symmetry. Refinement of our model, for example by increasing side chain flexibility or introducing type 3 bead self-attraction, may switch the effective potential into a preferential *pm3m* cubic symmetry state by softening it or making it more attractive, though on the other hand, may destroy the very factors that drive spherical unit coassembly. In a sense, we are faced with the very same factors experimentalists wrestle with in polyphilic liquid crystal design, with a slight advantage of being able to straightforwardly quantify all energetic structural contributions.

Finally, one of the most striking features of this work is the realisation of a global phase diagram for dendrons which shows the relation between the columnar and the supramolecular sphere phases. Whilst at a fixed P and T a change in molecular morphology is used empirically to drive the formation of a particular mesophase, here we suggest that these phases are related and changes in the thermodynamic state conditions may induce the appearance of unexpected mesophases.

Acknowledgements

Financial support for this work has been given by the U.K. Engineering and Physical Sciences Research Council (EPSRC), grant EP/E016340, "Molecular Systems Engineering". The authors are grateful for insights and fruitful discussions with John Seddon and Goran Ungar.

References

1 I. W. Hamley, *Angew. Chem., Int. Ed.*, 2003, **42**, 1692–1712.
2 J. M. Lehn, *Proc. Natl. Acad. Sci. U. S. A.*, 2002, **99**, 4763–4768.
3 T. Kato, N. Mizoshita and K. Kishimoto, *Angew. Chem., Int. Ed.*, 2006, **45**, 38–68.
4 C. Tschierske, *Chem. Soc. Rev.*, 2007, **36**, 1930–1970.
5 T. Kato, *Science*, 2002, **295**, 2414–2418.
6 P. J. Collings and M. Hird, *Introduction to Liquid Crystals*, Taylor & Francis, London, 1997.
7 K. A. Dill, *Protein Sci.*, 1999, **8**, 1166–1180.
8 K. Rajagopal and J. P. Schneider, *Curr. Opin. Struct. Biol.*, 2004, **14**, 480–486.
9 J. S. Rowlinson and F. L. Swinton, *Liquids and Liquid Mixtures*, Butterworths, London, 3rd edn, 1982.
10 D. L. Gin, X. Lu, P. R. Nemade, C. S. Pecinovsky, Y. Xu and M. Zhou, *Adv. Funct. Mater.*, 2006, **16**, 865–878.
11 V. Percec, M. Glodde, T. K. Bera, Y. Miura, I. Shiyanovskaya, K. D. Singer, V. S. K. Balagurusamy, P. A. Heiney, I. Schnell, A. Rapp, H. W. Spiess, S. D. Hudson and H. Duan, *Nature*, 2002, **419**, 384–387.
12 K. K. Ewert, H. M. Evans, A. Zidovska, N. F. Bouxsein, A. Ahmad and C. R. Safinya, *J. Am. Chem. Soc.*, 2006, **128**, 3998–4006.
13 D. J. P. Yeardley, G. Ungar, V. Percec, N. H. Holerca and G. Johansson, *J. Am. Chem. Soc.*, 2000, **122**, 1684–1689.
14 X. Zeng, G. Ungar, Y. Liu, V. Percec, A. E. Dulcey and J. K. Hobbs, *Nature*, 2004, **428**, 157–160.
15 V. Percec, W. D. Cho and G. Ungar, *J. Am. Chem. Soc.*, 2000, **122**, 10273–10281.
16 V. Percec, C. M. Mitchell, W. D. Cho, S. Uchida, M. Glodde, G. Ungar, X. Zeng, Y. Liu, V. S. K. Balagurusamy and P. A. Heiney, *J. Am. Chem. Soc.*, 2004, **126**, 6078–6094.
17 V. Percec, W. D. Cho, G. Ungar and D. J. P. Yeardley, *J. Am. Chem. Soc.*, 2001, **123**, 1302–1315.
18 V. Percec, W. D. Cho, P. E. Mosier, G. Ungar and D. J. P. Yeardley, *J. Am. Chem. Soc.*, 1998, **120**, 11061–11070.
19 V. Percec, W. D. Cho, G. Ungar and D. J. P. Yeardley, *Angew. Chem., Int. Ed.*, 2000, **39**, 1598–1602.
20 V. Percec, M. Peterca, M. J. Sienkowska, M. Ilies, E. Aqad, J. Smidrkal and P. A. Heiney, *J. Am. Chem. Soc.*, 2006, **128**, 3324–3334.
21 V. Percec, N. H. Holerca, S. Uchida, W. D. Cho, G. Ungar, Y. Lee and D. J. P. Yeardley, *Chem.–Eur. J.*, 2002, **8**, 1106–1117.
22 G. Ungar, V. Percec, N. H. Holerca, G. Johansson and J. A. Heck, *Chem.–Eur. J.*, 2000, **6**, 1258–1266.
23 V. Percec, A. E. Dulcey, M. Peterca, M. Ilies, S. Nummelin, M. J. Sienkowska and P. A. Heiney, *Proc. Natl. Acad. Sci. U. S. A.*, 2006, **103**, 2518–2523.
24 V. Percec, G. Johansson, J. A. Heck, G. Ungar and S. V. Batty, *J. Chem. Soc., Perkin Trans. 1*, 1993, 1411–1420.
25 V. Percec, G. Johansson, G. Ungar and J. Zhou, *J. Am. Chem. Soc.*, 1996, **118**, 9855–9866.
26 M. R. Rosen, C. J. Wilson, D. A. Wilson, M. Peterca, M. R. Imam and P. Percec, *Chem. Rev.*, 2009, **109**, 6275–6540.
27 V. S. K. Balagurusamy, G. Ungar, V. Percec and G. Johansson, *J. Am. Chem. Soc.*, 1997, **119**, 1539–1555.
28 M. R. Wilson, *Chem. Soc. Rev.*, 2007, **36**, 1881–1888.
29 E. A. Müller and L. D. Gelb, *Ind. Eng. Chem. Res.*, 2003, **42**, 4123–4131.
30 W. Shinoda, R. Devane and M. L. Klein, *Mol. Simul.*, 2007, **33**, 27–36.
31 C. Avendaño, T. Lafitte, A. Galindo, C. S. Adjiman, G. Jackson, and E. A. Müller, Coarse-Grained SAFT-γ Mie force field for molecular simulation, 2011, in preparation.
32 (*a*) S. Izvekov and G. A. Voth, *J. Phys. Chem. B Lett.*, 2005, **109**, 2469–2473; (*b*) S. Izvekov and G. A. Voth, *J. Chem. Phys.*, 2005, **123**, 134105.
33 S. O. Nielsen, C. F. Lopez, G. Srinivas and M. L. Klein, *J. Phys.: Condens. Matter*, 2004, **16**, R481–R512.
34 M. McCullagh, T. Prytkova, S. Tonzani, N. D. Winter and G. C. Schatz, *J. Phys. Chem. B*, 2008, **112**, 10388–10398.

35 C. Avendaño and E. A. Müller, *Phys. Rev. E: Stat., Nonlinear, Soft Matter Phys.*, 2009, **80**, 061702.
36 C. Avendaño and E. A. Müller, *Soft Matter*, 2011, **7**, 1694–1701.
37 M. A. Horsch, Z. Zhang and S. C. Glotzer, *Soft Matter*, 2010, **6**, 945–954.
38 A. Alsunaidi, W. K. den Otter and J. H. R. Clarke, *J. Chem. Phys.*, 2009, **130**, 124910.
39 A. J. Crane, F. J. Martínez-Veracoechea, F. A. Escobedo and E. A. Müller, *Soft Matter*, 2008, **4**, 1820–1829.
40 A. J. Crane and E. A. Müller, *Faraday Discuss.*, 2010, **144**, 187–202.
41 A. J. Crane and E. A. Müller, *J. Phys. Chem. B*, 2011, **115**, 4592–4605.
42 T. C. Nguyen, Z. Zhang and S. C. Glotzer, *J. Chem. Phys.*, 2008, **129**, 244903.
43 J. J. K. Kirkensgaard and S. Hyde, *Phys. Chem. Chem. Phys.*, 2009, **11**, 2016–2022.
44 J. D. Weeks, D. Chandler and H. C. Andersen, *J. Chem. Phys.*, 1971, **54**, 5237–5247.
45 W. G. Chapman, K. E. Gubbins, G. Jackson and M. Radosz, *Fluid Phase Equilib.*, 1989, **52**, 31–38.
46 E. A. Müller and K. E. Gubbins, *Ind. Eng. Chem. Res.*, 2001, **40**, 2193–2211.
47 C. Dellago and W. Lechner, *J. Chem. Phys.*, 2008, **129**, 114707.
48 P. J. Steinhardt, D. R. Nelson and R. Ronchetti, *Phys. Rev. B*, 1983, **28**, 784–805.
49 www.ccp5.ac.uk/DL_POLY/. For a recent review see W. Smith, *Mol. Simul.*, 2006, **32**, 933–1121.
50 F. J. Martínez-Veracoechea and E. A. Müller, *Mol. Simul.*, 2005, **31**, 33–43.
51 D. A. Kofke, *Mol. Phys.*, 1993, **78**, 1331–1336.
52 D. A. Kofke, *J. Chem. Phys.*, 1993, **98**, 4149–4162.
53 A. J. Crane, *Coarse-Grained Simulations of the Self-Assembly and Mesophase Behaviour of Polyphilic Liquid Crystals*, PhD thesis, Imperial College London, 2010.
54 A. K. Soper, *Chem. Phys.*, 1996, **202**, 295–306.
55 W. Schommers, *Phys. Lett. A*, 1973, **43**, 157–158.
56 A. P. Lyubartsev and A. Laaksonsen, *Phys. Rev. E.*, 1995, **52**, 3730–3737.
57 R. L. McGreevy and L. Pusztai, *Mol. Simul.*, 1988, **1**, 359–367.
58 R. L. Henderson, *Phys. Lett. A*, 1974, **49**, 197–198.
59 C. G. Gray and K. E. Gubbins, *Theory of Molecular Fluids*, Oxford University Press, Oxford, 1984.
60 G. Brannigan, A. C. Tamboli and F. L. H Brown, *J. Chem. Phys.*, 2004, **121**, 3259–3271.
61 O. Farago and N. Gronbech-Jensen, *J. Am. Chem. Soc.*, 2009, **131**, 2875–2881.

